Wang *et al. Earth, Planets and Space* (2018) 70:59
https://doi.org/10.1186/s40623-018-0821-9

Earth, Planets and Space

FULL PAPER

Open Access

Spread-F occurrences and relationships with foF2 and h′F at low- and mid-latitudes in China

Ning Wang[1,2*], Lixin Guo[1], Zhenwei Zhao[2], Zonghua Ding[2] and Leke Lin[2]

Abstract

Ionospheric irregularities are an important phenomenon in scientific studies and applications of radio-wave propagation. Spread-F echoes in ionograms are a type of high-frequency band irregularities that include frequency spread-F (FSF), range spread-F (RSF), and mixed spread-F (MSF) events. In this study, we obtained spread-F data from four ionosondes at low- and mid-latitudes near the 120°E chain in China during the 23rd solar cycle. We used these data to investigate spread-F occurrence percentages and variations with local time, season, latitude, and solar activity. The four ionosondes were located at Haikou (HK) (20°N, 110.34°E), Guangzhou (GZ) (23.14°N, 113.36°E), Beijing (BJ) (40.11°N, 116.28°E), and Changchun (CC) (43.84°N, 125.28°E). We also present possible correlations between spread-Fs and other ionospheric parameters, such as the critical frequency of the F2-layer (foF2) and the virtual height of the bottom-side F-layer (h′F). In particular, we investigated the possible threshold of the foF2 affecting the FSF and the relationship between the h′F and the RSF. The main conclusions are as follows: (a) the FSF occurrence percentages were anti-correlated with solar activity at all four sites; meanwhile, RSF occurrence rates increased with the increase in solar activity at HK, but not at the other three sites; (b) FSF occurrence rates were larger at the mid-latitudes than expected, while FSFs occurred more often after midnight; (c) the highest FSF occurrence rates mostly appeared during the summer months, while RSFs occurred mostly in the equinoctial months of 2000–2002 at HK and GZ; (d) a lower foF2 was suitable for FSF events; nevertheless, h′F and RSF occurrences satisfied the parabolic relationship; (e) the foF2 thresholds for FSFs were 15, 14, 7.6, and 7.8 MHz at HK, GZ, BJ, and CC, respectively. The h′Fs occurring between 240 and 290 km were more favorable for RSF occurrences. These results are important for understanding ionospheric irregularity variations in eastern Asia and for improving space weather modeling and forecasting capabilities .

Keywords: Ionospheric irregularities, Spread-F occurrence percentage, foF2 threshold for FSF, Relationship between h′F and RSF

Introduction

In the middle to late 1930s, ionospheric irregularities and the manner in which their electrodynamic mechanisms affected ionospheric behaviors began to attract the interest of many researchers (Abdu et al. 1981a, b, 1998, 2009; Booker and Wells 1938; Bowman 1974, 1990; Chandra and Rastogi 1970; Chou and Kuo 1996; de Jesus et al. 2013; Ossakow 1981; Xiong et al. 2012). Ionospheric irregularities appear as scattered echoes in high-frequency (HF) band ionograms that are known as spread-F events. Spread-Fs can manifest as frequency spread-Fs (FSF) that are broadened traces that mark reflections from the ionosphere along the frequency axis, or as range spread-Fs (RSF) that are along the vertical height axis. Many ground-based instruments (optical, ionosondes, and radar) and space-borne platforms (rockets and satellites) have been employed to explore the spread-F phenomenon over the past seven decades. These efforts have deepened our knowledge on spread-Fs showing that they vary with respect to latitude, local time, season, and solar and magnetic activity (Alfonsi et al. 2013; Banola et al. 2005;

*Correspondence: wn_22s_cetc@163.com
[1] School of Physics and Optoelectronic Engineering, Xidian University, Xi'an, Shaanxi 710071, China
Full list of author information is available at the end of the article

Chou and Kuo 1996; Deng et al. 2013; Huang et al. 1993; Scherliess and Fejer 1999). Different mechanisms have been proposed to explain spread-F occurrences and their development (Bowman 1990; Fejer et al. 1999; Fukao et al. 2004); among these, the primary mechanism in equatorial regions is the generalized Rayleigh–Taylor (R–T) instability mechanism. The R–T instability mechanism suggests that pre-reversal electric field enhancements (PRE) during the evening cause a rapid uplift of the ionosphere's F-layer (Fejer et al. 1999; Fukao et al. 2004; Manju et al. 2007; Sukanta et al. 2017; Xiong et al. 2012; Upadhayaya and Gupta 2014). Relationships between spread-Fs and other ionospheric parameters, particularly the F2-layer (foF2) and h′F variations with the occurrence of spread-Fs, have also been statistically examined (Rungraengwajiake et al. 2013; Joshi et al. 2013; Madhav Haridas et al. 2013; de Abreu et al. 2014a, b, c, 2017; Abadi et al. 2015; Manju and Madhav Haridas 2015; Smith et al. 2015; Liu and Shen 2017). In addition, the effects of seasonal, solar, and magnetic activity variabilities on the h′F threshold have also been investigated (Manju et al. 2007; Manju and Madhav Haridas 2015; Madhav Haridas et al. 2013; Stoneback et al. 2011; Narayanan et al. 2014, 2017).

Devasia et al. (2002) first introduced the concept of threshold height (h′Fc) as a critical parameter controlling the day-to-day equatorial spread-F (ESF) variability. Past studies have revealed the dependence of the h′Fc on seasonal variations and solar and magnetic activity for the occurrence of ESFs and found the occurrences to be irrespective of the magnitude and polarity of meridional winds (Jyoti et al. 2004; Manju et al. 2007). Rungraengwajiake et al. (2013) presented a comparative study of the correlation between h′F and RSF occurrences in Thailand, and the results showed that high RSF occurrences mostly happened during equinoctial months that corresponded to rapid increases in the monthly mean h′F after sunset. Joshi et al. (2013) found that the h′F plays a key role in determining the R–T instability growth rate. Madhav Haridas et al. (2013) presented the effects of seasonal and solar activity variations of the h′Fc on ESF occurrences in India and found that substantial increases in the h′Fc varied with magnetic activity during every season.

Similar studies in Brazil have been presented (de Abreu et al. 2014a, b, c) to show that the occurrence of ESFs are closely related to daily variations of the h′F near the equator. During periods of low solar activity (LSA), the 250 km h′F altitude acted as the h′Fc for the generation of spread-Fs, while the 300 km h′Fc was during periods of high solar activity (HSA). An investigation using measurements from multiple instruments over the American sector showed that spread-Fs were often observed the nights before and during storms near the equator, in which the foF2 was less than 8 MHz and the h′F was lower than 300 km (de Abreu et al. 2017).

Abadi et al. (2015) studied the influences of the h′F on the latitudinal extension of ionospheric irregularities in Southeast Asia. Their results suggested that the latitudinal extension of plasma bubbles was mainly controlled by the PRE magnitude and h′F peak values during the initial phases of the ESF. Manju and Madhav Haridas (2015) investigated the h′Fc for the occurrences of ESFs during equinoxes and showed that the equinoctial asymmetry of the h′Fc increases with solar activity. Aside from the studies mentioned above, there are few reports that consider the effect of the foF2 threshold on the generation of spread-F events. Liu and Shen (2017) conducted a case study during a severe geomagnetic storm near 120°E in China and showed that the spread-F was suppressed near Sanya and Wuhan during the storm's main phase when the frequency spread over 14 MHz, and the suppression was sustained for several hours. This helped us to understand the possible onset causes of the day-to-day spread-F variability.

Stoneback et al. (2011) investigated the local time distribution of meridional (vertical) drifts during the prolonged solar minimum. They found that the downward drifts across sunset and the upward drifts across midnight were also consistent with the delay in the appearance of ionospheric irregularities after midnight. Narayanan et al. (2014) studied the relationship between the occurrence of satellite traces (STs) in ionograms and the formation of ESFs using observations from an Indian dip equatorial station during solar minimum conditions. They found that the ST occurred later in the night as well implying that the PRE was not the cause of the ST during these times. Additionally, they also found that the STs were not followed by ESFs in about 30% of the cases indicating that large-scale wave-like structures (LSWS) do not trigger ESFs on all occasions. Narayanan et al. (2017) also found that the plasma bubbles were generated without strong PREs when the ion-neutral collision frequencies possibly dropped significantly during the unusually low solar activity conditions of 2008. Abdu et al. (2006) found that the existence of significant planetary wave (PW) influences on plasma parameters at E- and F-region heights over the equatorial latitudes using airglow, radar, and ionospheric sounding observations. A direct consequence of the PW scale oscillations in the evening electric field is its role in the quiet time day-to-day variability of the ESF/plasma bubble occurrences and intensities.

We limited our focus to spread-F occurrences and their relationships with foF2 and h′F that affected spread-F occurrences during a complete solar cycle in the low- and mid-latitudes over China. The International Reference Ionosphere-2012 (IRI-2012) model includes the monthly

mean spread-F occurrences for predicting in the Brazilian longitude sector but not for Chinese sector. Therefore, the studies of spread-F occurrence statistics in China are part of an on-going effort to develop the spread-F occurrence prediction abilities to improve the IRI model. In the present study, we focused on the characteristics and correlations between spread-F occurrences and the foF2 and h′F. Furthermore, we also present the thresholds of the foF2 as they relate to the generation of FSFs.

Data and analysis

The China Research Institute of Radio-wave Propagation (CRIRP) constructed and operated a network of long-running ionospheric observation sites that cover mainland China. In this study, we extracted simultaneous spread-F data from four digital ionosondes located at Haikou (HK) (20°N, 110.34°E), Guangzhou (GZ) (23.14°N, 113.36°E), Beijing (BJ) (40.11°N, 116.28°E), and Changchun (CC) (43.84°N, 125.28°E). In addition, we also determined the data characteristic of the foF2 and h′F at these sites to reveal possible correlations between spread-F occurrences and the foF2 and h′F. No data were recorded in December 1997 and from May to December 1999 at CC, because the ionosonde was being repaired. The observational site details are shown in Table 1.

The HK and GZ sites lie near the north crest of the equatorial ionization anomaly (EIA) zone. The EIA zone is where the fountain effect phenomena and the equatorial electrojet often interact resulting in complicated ionospheric physical processes. BJ and CC are located at the mid-latitudes in China. According to previous studies, ionospheric irregularities greatly depend on solar activity, local time, season, latitude and longitude, and geomagnetic disturbances (Abdu et al. 1981a, b, 1983, 1998, 2009; Booker and Wells 1938; Bowman 1974; Chandra and Rastogi 1970; Maruyama 1988; Xiong et al. 2012). To discuss the correlations between spread-Fs and solar and geomagnetic activities, we show the monthly mean 10.7 cm radio flux (F10.7) and ap index during the 23rd solar cycle in Fig. 1 that covers the epochs of the LSA and HSA. We used a 3-hourly ap index to identify geomagnetically quiet and disturbed days. If the maximum value of the 3-hourly ap index for a day was greater than 12, the day was considered as a disturbed day (Narayanan et al. 2017). Figure 2 shows the daily max ap indices from 2000 to 2005. Further, it can be seen from the figure that there were more geomagnetically disturbed days during the vernal equinox and autumn equinoxes in 2001 and 2002.

Ionogram data were collected using type TYC-1 ionosondes, which are designed and manufactured by the CRIRP (Xu et al. 2001). Ionograms were recorded at 1-h intervals for a frequency range from 1 to 32 MHz. We distinguished two types of spread-F, FSF, and RSF for detailed study. We used the percentage of spread-F occurrences to describe the spread-F statistical features, which is defined as follows:

$$\mathrm{P}(y,m,h) = \frac{n(y,m,h)}{N(y,m,h)} \times 100\% \quad (1)$$

where y, m, and h represent the year, month, and local time (LT), respectively; n is the number of spread-F occurrences that appear at the same local time but during different days of a single month, and N is the total number of days for a given year and local time. Spread-Fs typically appeared after sunset and lasted until the subsequent sunrise; thus, the percentage of spread-F occurrences from 18:00 LT to 06:00 LT is the topic of interest in this study. Occurrences of FSF and RSF were compared with monthly medians of the foF2 and h′F to find the correlations between foF2 and h′F for the generation of spread-Fs. The FSF, RSF, foF2, and h′F were differentiated by manually analyzing the ionograms. The foF2 and h′F can sometimes be measured, but sometimes cannot be obtained when a spread-F occurs. The foF2 and h′F cannot be obtained during a strong spread-F (SSF). SSFs are a type of spread-F that can be identified when there is strong diffusion on the frequency and height axis of an ionogram. Figure 3 shows a SSF event in Haikou on March 26, 2012. The observations presented in this manuscript contain data when the foF2 and h′F values were reliably scaled during a spread-F. To examine their seasonal variations, we grouped the data into the following four seasonal bins: summer (May, June, July and August), vernal equinox (March and April), autumn equinox (September and October), and winter (January, February, November and December) (Maruyama and Matuura 1984; Maruyama et al. 2009; Sripathi et al. 2011; Xiao and Zhang 2001).

Table 1 Details of the digital ionosonde sites used in the investigation

Location	Symbol used	Geog. Lat. (°N)	Geog. Long. (°E)	Geom. Lat. (°N)	Geom. Long. (°E)
Haikou	HK	20.00	110.34	10.02	182.45
Guangzhou	GZ	23.14	113.36	19.53	185.27
Beijing	BJ	40.11	116.28	30.22	187.51
Changchun	CC	43.84	125.28	34.26	195.21

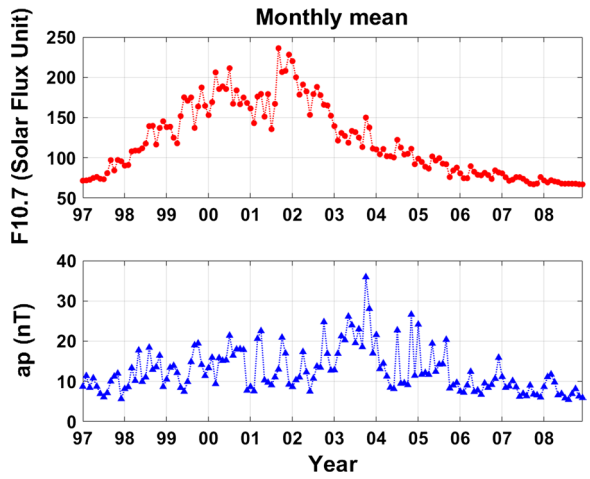

Fig. 1 Monthly averaged 10.7 cm solar flux (F10.7) (y axis: F10.7/sfu) and ap index from 1997 to 2008 denoting the solar activity

Results and discussion

Nocturnal, seasonal, and solar activity variations on spread-F occurrences

The monthly mean of the FSF occurrence rates varied with local time and are presented separately in Fig. 4 for Haikou, Guangzhou, Beijing, and Changchun. It can be found that the FSF occurrences frequently appeared after midnight. Also, the FSF occurrences observed at different sites exhibited distinct local time distribution patterns. Previous studies have also observed this trend (Zhang et al. 2015; de Jesus et al. 2010, 2012, 2016). The FSF occurrence rates at HK, BJ and CC were higher than GZ. The maximum FSF occurrence rate was ~ 80% and occurred in July 1997 at HK, in August 2008 at BJ and in June 2006 at CC. The LSA yielded high FSF occurrence percentages at all four sites. The relationship between the FSF and solar activity was approximate to a negative correlation. The seasonal variation of the FSF occurrence rates observed at the four sites is shown in Fig. 5a–d. We found that FSFs occurred mostly during the summer at HK and the occurrence rate was lower between 1999 and 2002. FSF occurrence rates were higher during the autumn equinox than during the vernal equinox between 2000 and 2001 at HK. FSFs occurred mostly during the summer at GZ, however, scarcely occurred in 2002 and 2008. Statistically, the FSFs started at approximately 21:00 LT and lasted until 05:00 LT at HZ and CC. However, FSFs started at about 23:00 LT and lasted until 05:00 LT at GZ and BJ, with post-midnight FSFs as the most commonly observed.

Figure 6 shows variations in the average RSF occurrence rates at the four sites. The RSF occurrence rate was much larger than the FSF occurrence rate at GZ; however, the rates were smaller than the FSF occurrence rates at BJ and CC. RSF occurrence rates increased with an increase in solar activity at HK, but not at the other three sites. The maximum RSF occurrence rate was higher than 80% in June 2006 and July 2007 at GZ. Figure 7 shows the seasonal RSF occurrence rate variations at the four sites. RSFs mostly occurred in the vernal equinox and autumn equinox months during HSA years at HK and GZ. These observations revealed that the RSF occurrence rate from 2000 to 2002 at HK and GZ were possibly affected by the geomagnetic activity according to Fig. 2. During the solar

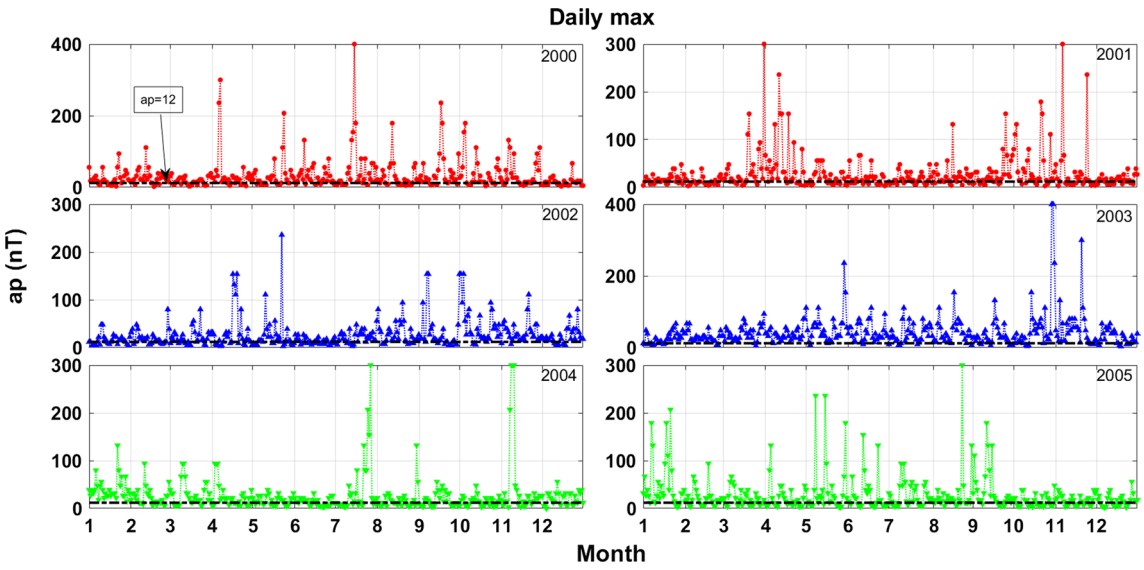

Fig. 2 Daily max ap indices from 2000 to 2005

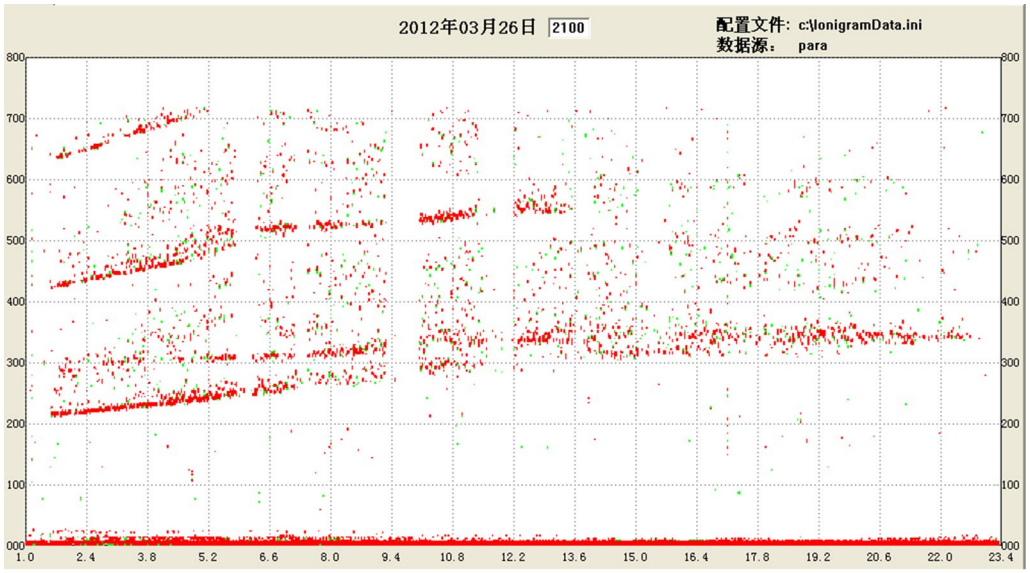

Fig. 3 A SSF event in Haikou on March 26, 2012

maximum period between 2000 and 2002, RSFs appeared earlier than during other periods, with a maximum RSF occurrence rate occurring between 21:00 LT and 01:00 LT at HK and GZ. Different from the FSF occurrences, higher RSF occurrence rates mostly occurred during the winter months at BJ and CC. Previous studies have emphasized that FSF events are well correlated with bottom-side layers, while RSFs are closely correlated with plumes. Additionally, the RSF occurrence rate reaches its maximum before midnight during HSA at low latitude, whereas that of an FSF reaches a maximum after midnight (Liu et al. 2004a, b; Chen et al. 2006; Aarons et al. 1994; Hu et al. 2004). This regular pattern was also observed at the four sites in China.

Abdu et al. (2003) showed that RSF events are associated with developed or developing plasma bubble events, while FSF events are associated with narrow-spectrum irregularities that occur near the peak of the F-layer. These results suggest that the upward velocity of plasma bubbles have a strong seasonal connection with the maximum values observed during the summer. Variations of FSF and RSF except for those during the 2000–2002 solar maximum period are mainly consistent with these studies. Rungraengwajiake et al. (2013) showed that FSF events appear later than RSF events on average and that FSFs remain until morning, while RSFs almost disappear by around 04:00 LT. The results shown in Figs. 5 and 7 are slightly different, which may be partly attributed to the effects of geomagnetic activity. Figure 2 shows the geomagnetic activity during the equinoxes in 2001 and 2002. It is possible these activities caused the RSFs to occur mainly during equinoxes at HK and GZ in 2001 and 2002. The peak FSF occurrence rate appeared later at GZ than at HK, which is well correlated with the manner in which fresh bubbles start from the latter station and then expand to high latitudes. The average FSF occurrence percentage mostly peaks from 24:00 LT to 02:00 LT at HK and from 03:00 LT to 05:00 LT at GZ. The average RSF occurrence percentages mostly peaked from 21:00 LT to 23:00 LT at HK and from 24:00 LT to 02:00 LT at GZ during periods of HSA. Meanwhile, RSF occurrence rates were higher at HK and GZ than those at BJ and CC; FSF occurrence rates were higher at HK, BJ, and CC than at GZ. These results support the hypothesis that solar and geomagnetic activity affects seasonal and longitudinal variations of spread-Fs.

Liu and Shen (2017) found that the disturbance of electric fields could also contribute to the occurrence of spread-Fs, especially at low-latitude stations. The disturbed electric fields and the disturbance winds are also the probable factors that promote the spread-F along with the gravity-driven R–T instability. In addition, the electric field disturbances can also generate spread-Fs through R–T instability only (de Jesus et al. 2010; Wang et al. 2014; Wan and Xu 2014; Mo et al. 2017). The disturbance of the dynamo driven by enhanced global thermospheric circulation resulting from energy input at high latitudes is another factor for promoting spread-Fs (de Jesus et al. 2010; Liu and Shen 2017). Therefore, it can be seen that there are many possible mechanisms for spread-F occurrences, and more in-depth analysis is needed.

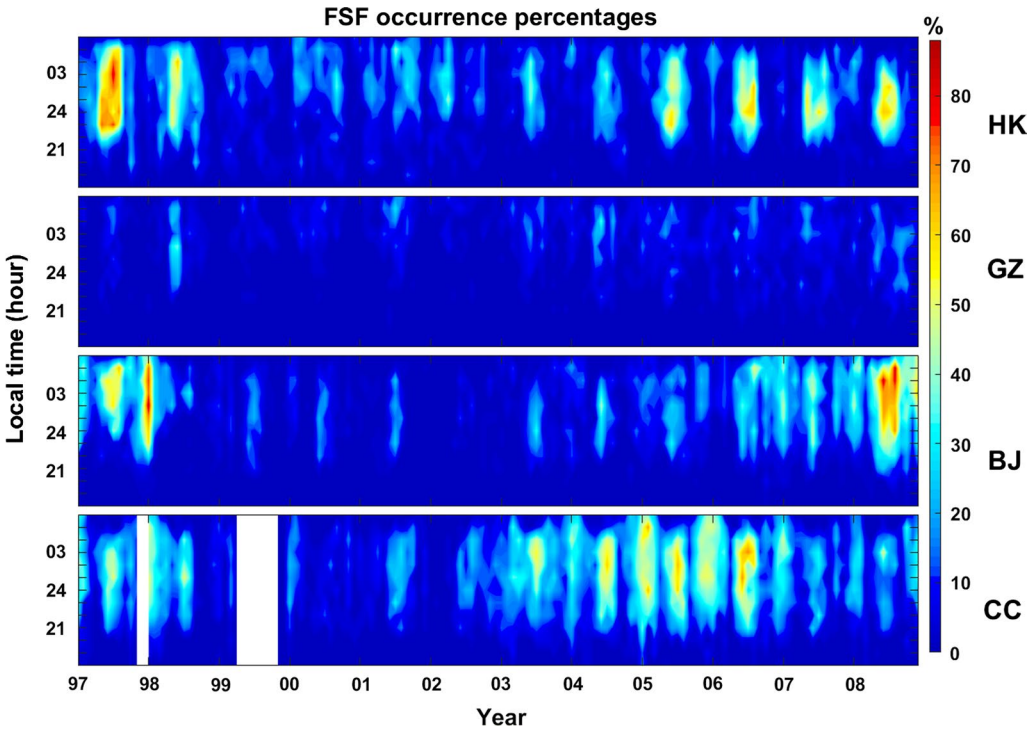

Fig. 4 Monthly mean FSF occurrence percentages at the four sites

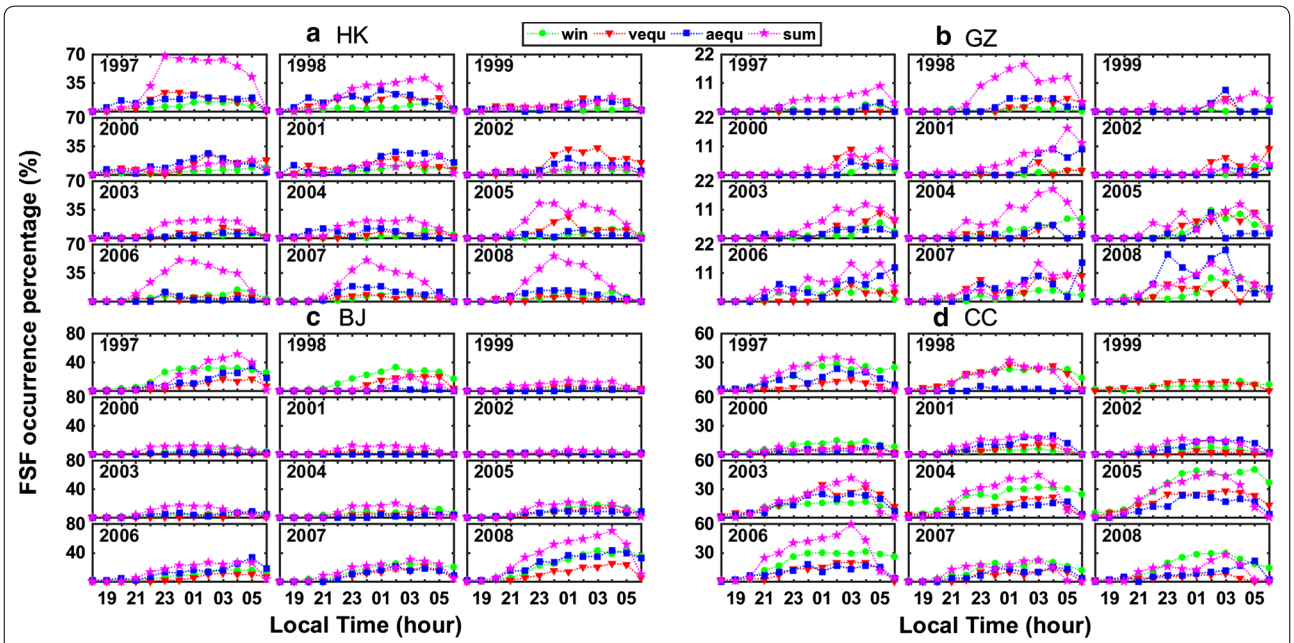

Fig. 5 Seasonal variation of the FSF occurrences observed at HK (**a**), GZ (**b**), BJ (**c**), and CC (**d**)

Nocturnal, seasonal, and solar activity variations on foF2 and h′F

In Fig. 8 we showed local time and the variations in solar activity in the monthly median foF2 data from the 23rd solar cycle. At lower latitudes, a higher magnitude foF2 was sustained until midnight. In addition, another morphological feature of the monthly medians is the typical post-sunset peak values. Between 1998 and 2005, foF2

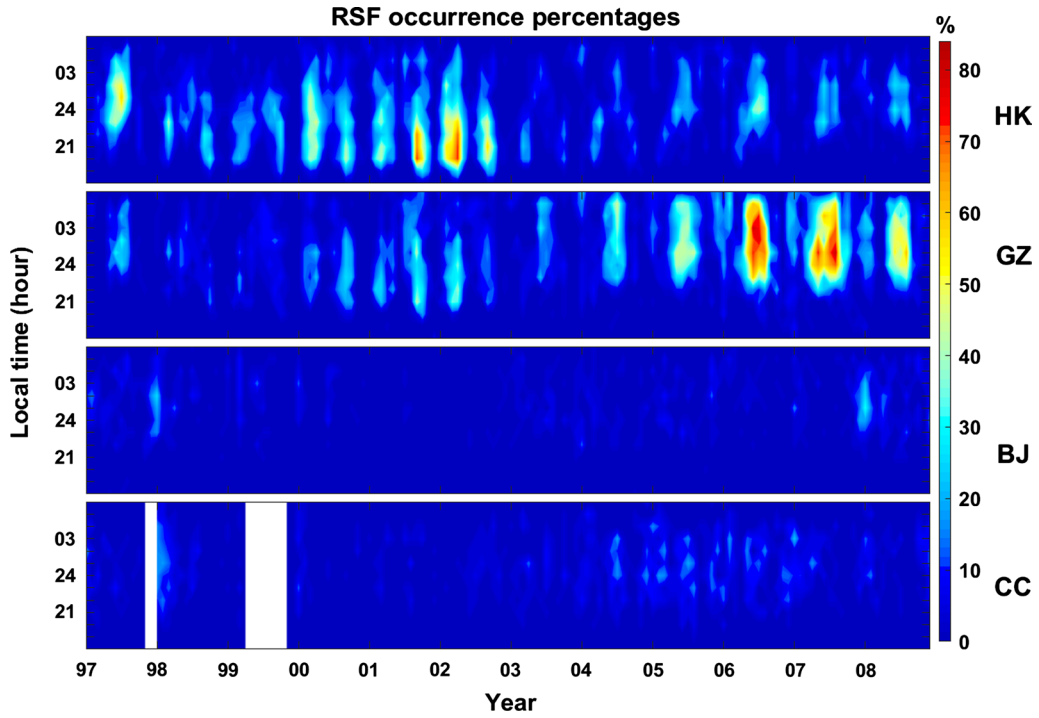

Fig. 6 Same as Fig. 2, but for the RSF occurrences

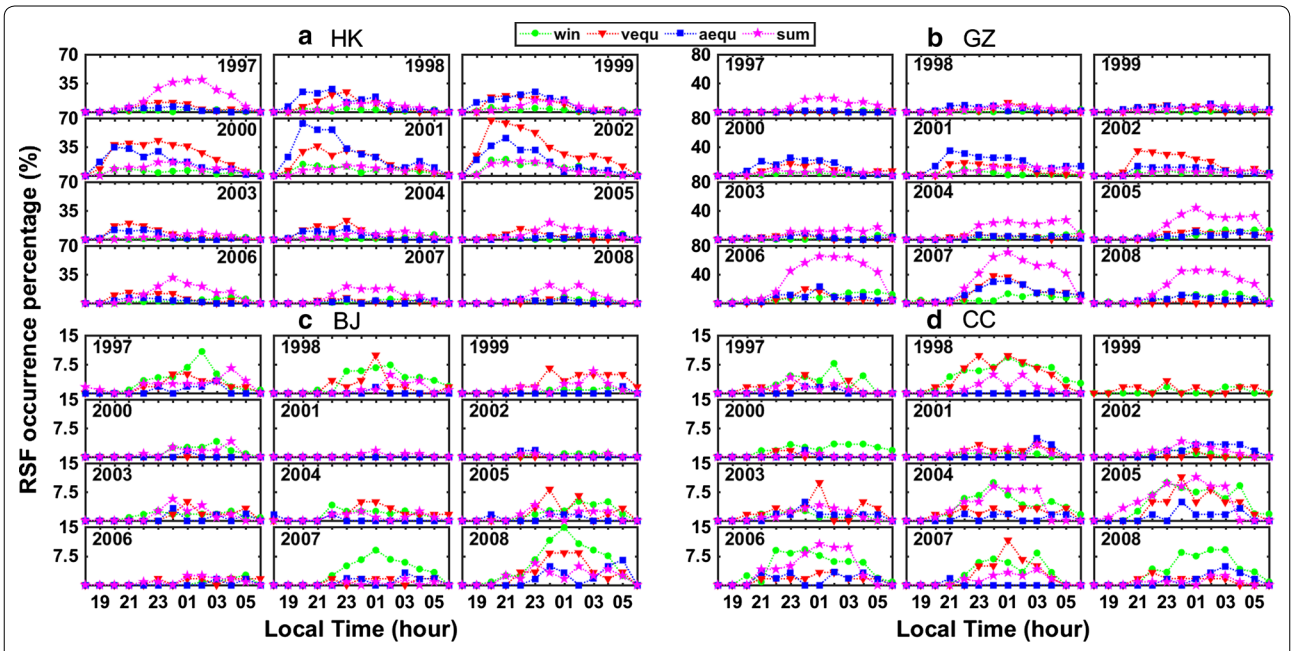

Fig. 7 Seasonal variation of the RSF occurrences at HK (**a**), GZ (**b**), BJ (**c**), and CC (**d**)

variations showed dual-peak patterns at HK and GZ that reached a minimum during the summer and a maximum during the spring and winter. Additionally, wintertime monthly medians of the foF2 were higher during the spring in 1998, but this result is inverted between 2003 and 2005. Figure 9 shows the seasonal variations of the

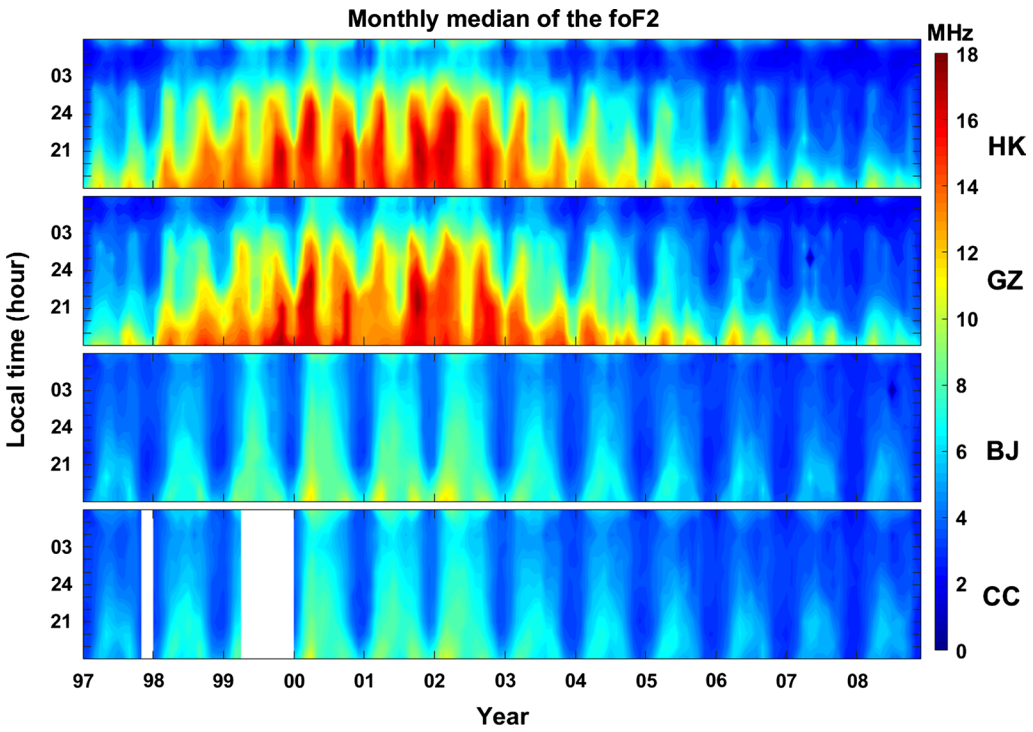

Fig. 8 Variation of the monthly median foF2 at the four sites between 1997 and 2008

averaged foF2 monthly median data at all four sites. The medians reached their peak magnitudes between 18:00 and 19:00 LT. In addition, the medians were mostly higher during equinox seasons at HK and GZ; however, they were mostly higher during the summer at BJ and CC. The highest foF2 medians were ~ 18 MHz and occurred from 18:00 LT to 24:00 LT at HK and GZ during periods of maximum solar activity. The minimal medians occurred before dawn from around 03:00–05:00 LT. The post-midnight collapse of the foF2 usually occurred more often at low latitudes than mid-latitudes.

Abdu et al. (1983) proposed that the h′F parameter may be a possible factor involved in the occurrence and variation of spread-Fs. Figure 10 shows the h′F monthly median data at all four sites, thus demonstrating that monthly medians were higher at HK and GZ than at BJ and CC. The peak median h′F values occurred before midnight during the summer in HSA at HK and GZ; however, the peak value onset time was later at high latitudes. During periods of HSA, monthly medians increase. Figure 11 shows the seasonal variation of the average h′F monthly median at the four sites, which is quite different from the foF2. The maximum h′F values occurred from 21:00 LT to 01:00 LT during summer months at HK and GZ; otherwise, they appeared at or before midnight from 2000 to 2002.

The possible foF2 threshold for FSFs and the relationship between the h′F and RSF

The correlations between spread-F occurrence and the foF2 and h′F magnitudes are discussed in this section. Figures 12 and 13 show the post-sunset foF2 and h′F variations compared with the normalized spread-F occurrence rates at the four sites. In order to analyze the correlation between the spread-F occurrence rate and the foF2 and h′F, the normalized probability was used. The normalized spread-F occurrence rate is defined as follows:

$$p_i = \frac{m_i}{\sum_i m_i} \tag{2}$$

$$\sum_i p_i = 1 \tag{3}$$

where p is the normalized FSF or RSF occurrence rate, m_i is the number of FSF or RSF event occurrences when the foF2 or h′F is within a certain interval. We used 0.2 MHz and 5 km as the sampling intervals for the foF2 and h′F. The summation of m_i is the total number of FSF or RSF event occurrences. We applied the polynomial fitting method during the relationship analysis between the foF2 and h′F and the spread-F occurrence rates. We found that the foF2 and FSF occurrences satisfy the linear relationship shown in Fig. 12, and the h′F and RSF occurrences

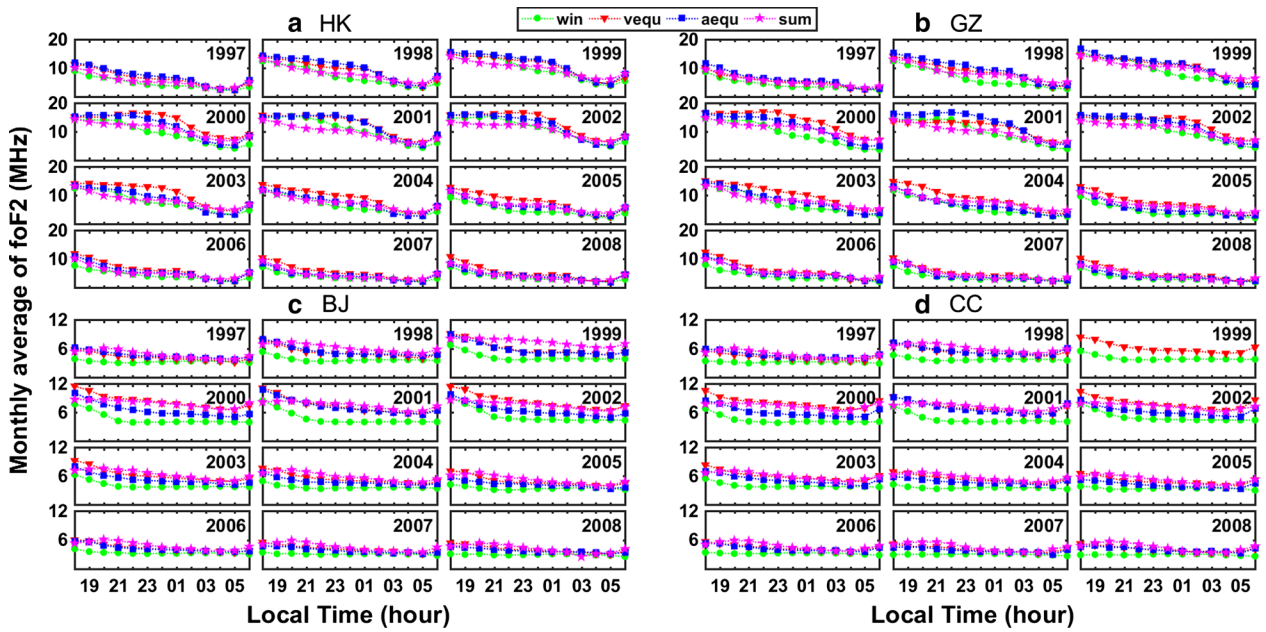

Fig. 9 Seasonal variation of the monthly median foF2 at HK (**a**), GZ (**b**), BJ (**c**), and CC (**d**)

are similar to parabolic relationship shown in Fig. 13. The red point is the sample value. The blue lines are a fitting line or curve. The FSF occurrence rates increased with a decrease in foF2 at each site, and the foF2 values ranged from 2.5 to 18 MHz at HK and GZ. A straight line is drawn when the normalized spread-F occurrence rate is equal to 0% as in Fig. 12. The intersection of this line and the blue line is considered the foF2 threshold. We estimated that the foF2 threshold at HK and GZ was ~ 15 and ~ 14 MHz because almost the FSF occurrence was ~ 0% when foF2 exceeded this magnitude. The foF2 values ranged from of 3–9 MHz at BJ and CC. Thus, the corresponding foF2 thresholds for BJ and CC were 7.6 and 7.8 MHz, respectively. It is evident that the foF2 variability was much larger at low latitudes than at mid-latitudes. There are few reports that consider the effect of the foF2 threshold on the generation of spread-F events. De Abreu et al. (2017) found that the spread-F was often observed during storms using measurements from multiple instruments over the American sector when the foF2 was below 8 MHz. De Abreu et al. (2017) showed that the post-sunset EIA is produced by the plasma fountain arising from the pre-reversal vertical drift enhancement in the F-region (as indicated by large sunset increases of h′F and decreases of foF2). Therefore, it can be seen that the rapidly changing Dst index will also affect spread-Fs; however, our research is not currently focused on ionospheric storms. The variation in foF2 at different latitudes suggests that the PRE is not the only factor to initiate FSFs. For example, the meridional wind can suppress the growth rate of the R–T instability, also attributing to the foF2 and FSF (Buonsanto and Titheridge 1987; Stoneback et al. 2011).

Figure 13 shows the post-sunset h′F variations compared with the RSF occurrence rates at the four sites. The red point is the sample value. The blue line is the fit curve. The RSF occurrence rate and the h′F satisfy the parabolic relationship. When the probability of the RSF was ~ 25% of the maximum probability of occurrence, we treated that virtual height value as the threshold value. The h′F occurring between 240 and 290 km is more favorable for RSF occurrence by calculation, which is different from the relationship between foF2 and FSF. Figures 6, 10, and 13 indicate that the higher occurrence rates of RSFs are well correlated with higher post-sunset h′F peaks (Rungraengwajiake et al. 2013). Previous studies observed spread-Fs in the equatorial region on nights when the h′F was below 300 km (Abadi et al. 2015; Manju and Madhav Haridas 2015; Liu and Shen, 2017; de Abreu et al. 2017). Our results also support this conclusion. In addition, Devasia et al. (2002), Jyoti et al. (2004) and Manju et al. (2007) obtained an h′F threshold for the spread-F occurrences in their studies in India. Devasia et al. (2002) found a threshold of about ~ 300 km for the cases in their study. Our results also show that when the virtual height is greater than 300 km, the probability of an RSF is very small. Jyoti et al. (2004) showed a linear relationship between solar activity and the h′F threshold.

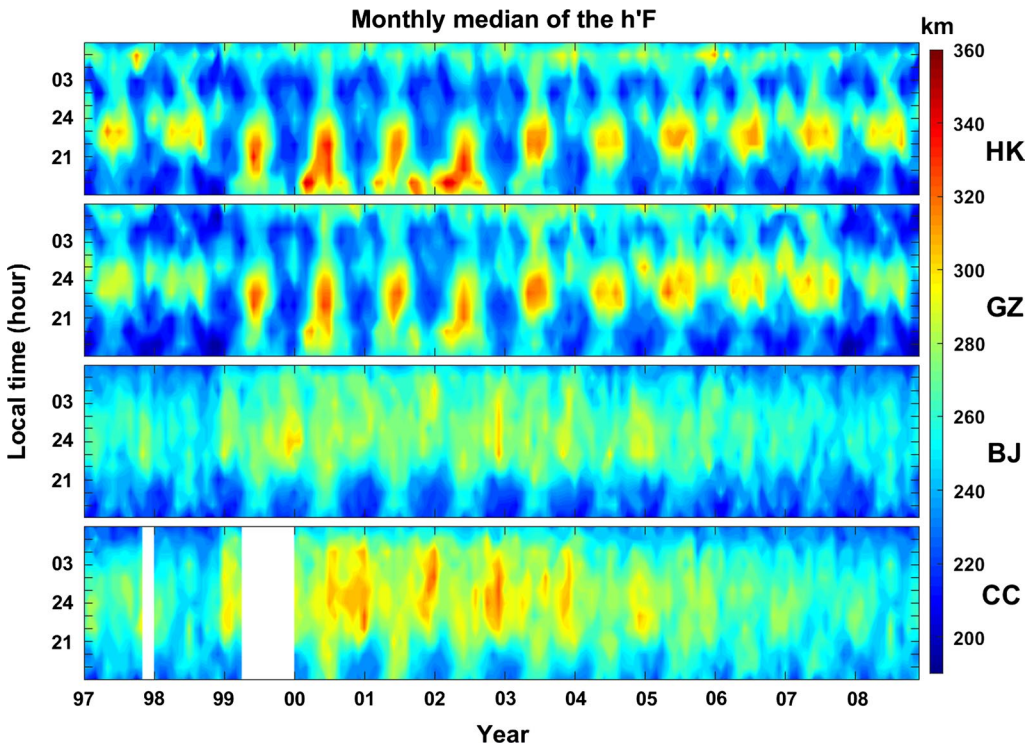

Fig. 10 Same as Fig. 6, but for monthly medians of the h′F

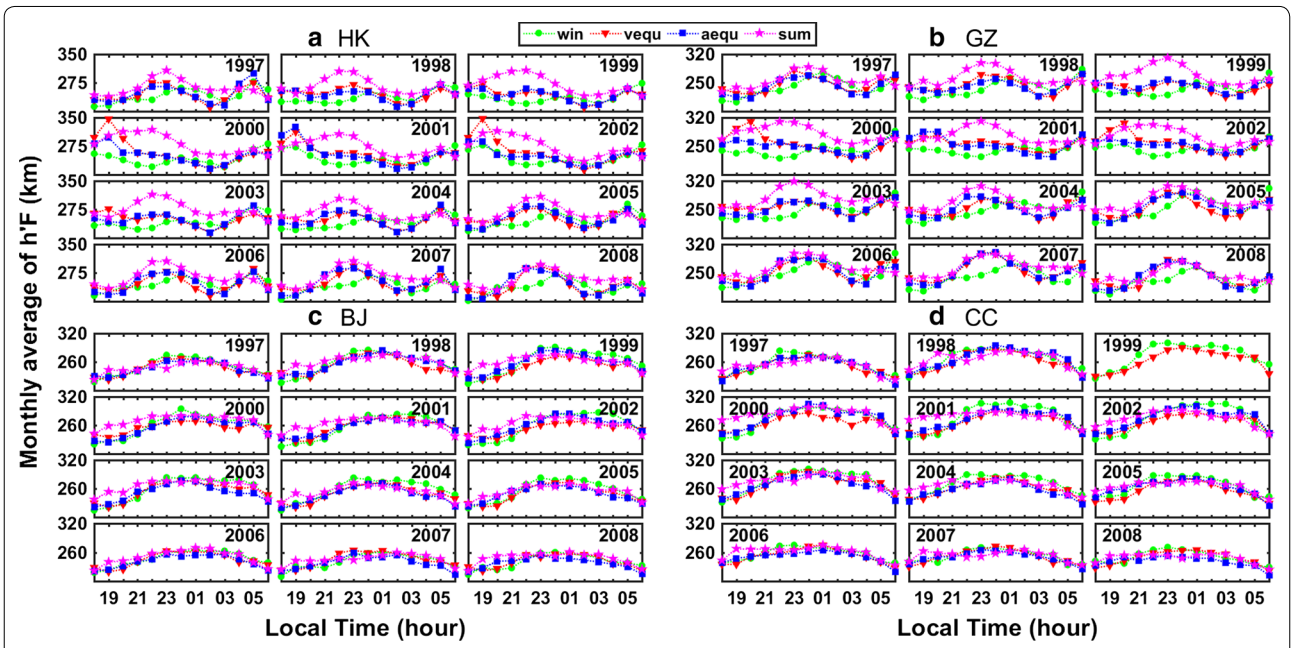

Fig. 11 Seasonal variation of the monthly medians of the h′F at HK (**a**), GZ (**b**), BJ (**c**), and CC (**d**)

Manju et al. (2007) investigated the dependence of the h′F threshold on seasonal and solar activity for magnetically quiet conditions and proposed the important role of neutral dynamics in controlling the day-to-day ESF variability. Abadi et al. (2015) found that latitudinal extension of plasma bubbles was mainly controlled by the h′F peak

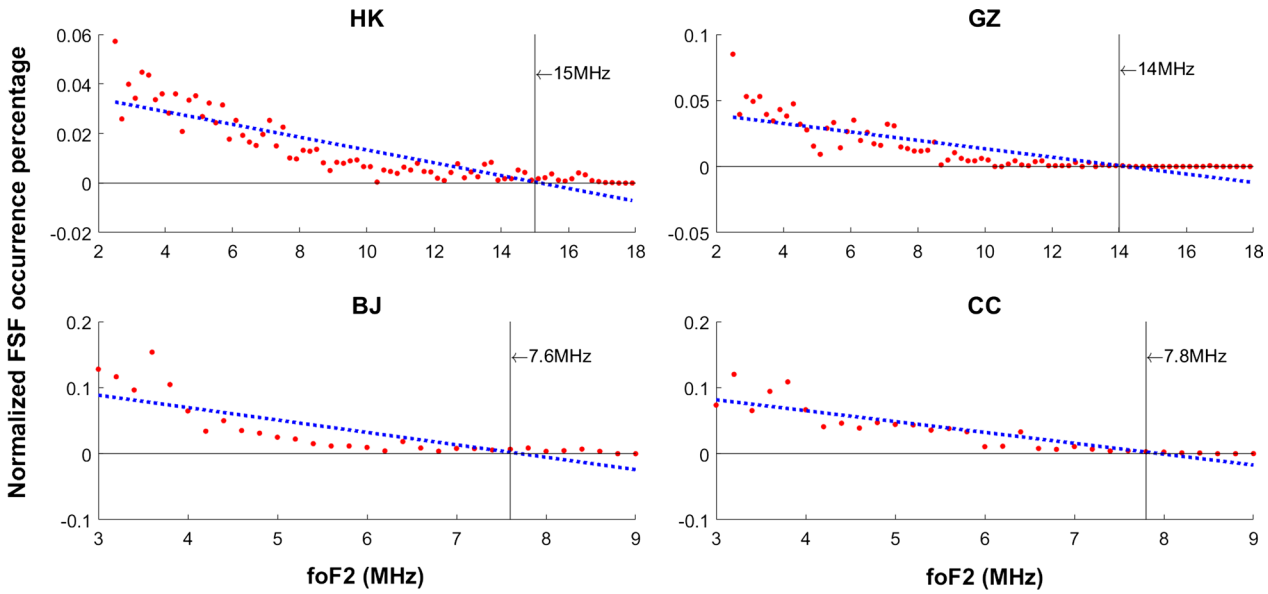

Fig. 12 Correlation between foF2 and the normalized FSF occurrence percentages

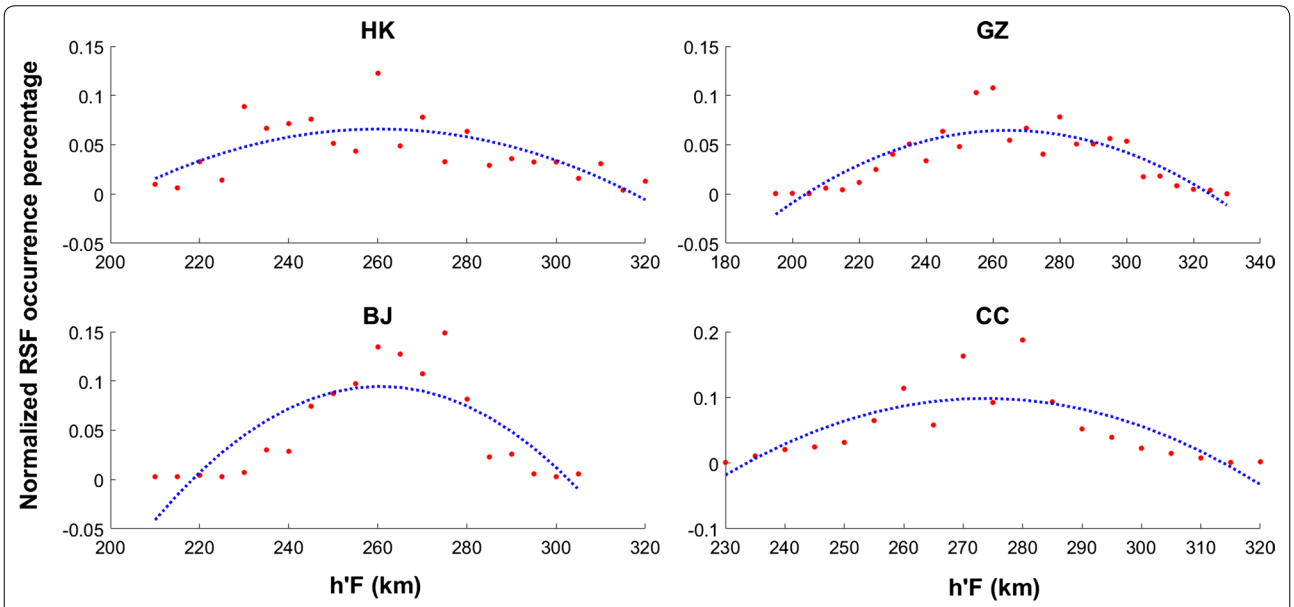

Fig. 13 Correlation between h′F and the normalized RSF occurrence percentages

value during the initial phase of an ESF. Manju and Madhav Haridas (2015) showed that the equinoctial asymmetry of the h′Fc increases with solar activity. In this article, the correlation between the h′F threshold and the seasonal and solar activities are not involved, and we will also focus on this content. The new idea presented from our study is the correlation between RSF occurrences and the h′F, which are different from previous research results. In a follow-up study, we will examine the relationship between the h′F threshold for RSFs and the solar and geomagnetic activities and equinoctial asymmetry.

The correlation RSF occurrence percentages with rapidly increasing post-sunset monthly mean h′F values substantiated the role of the PRE enhancement on RSF onsets. Traveling planetary wave ionospheric disturbance (TPWID)-type oscillations (de Abreu et al. 2014a, c; Fagundes et al. 2009) in the modulation of the

virtual height in the F-region increased during sunset hours. Meridional wind velocities corresponding to the post-sunset h′F for each spread-F event have been considered. Buonsanto and Titheridge (1987) found that the hmF2 dropped from 13:00 to 18:00 LT during the solar maximum periods because of the meridional wind. These results also indicate that the spread-F is a complex phenomenon, which implies that other possible factors can be ascribed to spread-F occurrences. The atmosphere ionosphere coupling process has been proposed as a contributing factor for spread-F development. Therefore, the connections between spread-F occurrence characteristics and the foF2 and h′F magnitudes deserve detailed investigation by additional theoretical and observational research. The foF2 and h′F thresholds also require further investigation using observations from different regions and under different solar activity conditions.

Summary and conclusions

In this study, we presented variations of the spread-F, foF2, h′F, the possible threshold of the foF2 for FSF, and the relationship between the h′F and RSF. The data in our study were recorded by four stations at low- and mid-latitudes near 120°E longitude in China during the 23rd solar cycle. The major conclusions are summarized as follows:

1. The FSF occurrence rates increased during years of LSA at all four sites. FSFs mainly occurred during the summer months, while RSFs occurred mostly in the equinoctial months between 2000 and 2002 at HK and GZ. Post-midnight FSFs were the most observed type of spread-F events. The typical FSF onset time was about 21:00 LT, and the FSFs normally lasted until 05:00 LT, while the RSFs occurred 2–3 h earlier at HK and GZ during periods of HSA.
2. The foF2 and h′F peak values come mainly before midnight at low latitudes, while h′F peak values appeared after midnight at mid-latitudes during periods of HSA.
3. Lower foF2 values were appropriate for FSF events; nevertheless, h′F and RSF occurrences satisfied the parabolic relationship. Most FSF events occurred when the foF2 was below 15 and 14 MHz at HK and GZ, and below 7.6 and 7.8 MHz at BJ and CC. The h′Fs occurring between 240 and 290 km were more favorable for RSF occurrences, which differ from the foF2. However, some questions remain unresolved and further studies are in progress.

Our studies of FSFs and RSFs in China are useful and have the potential to be included in the future IRI model. However, even after such studies of spread-F onsets and growth conditions, some uncertainties remain. This requires further efforts to understand the spread-F phenomenon at different locations. Soon, long irregularity data coverage over the China sector will be studied. More ionospheric parameters will be compared with local time and seasonal spread-F variations to amplify knowledge of the involved physical mechanisms.

Abbreviations

FSF: the frequency spread-F; RSF: the range spread-F; MSF: the mixed spread-F; foF2: the critical frequency of the F2-layer; h′F: the virtual height of the bottom-side F-layer; EIA: equatorial ionization anomaly; F10.7: the monthly average data of 10.7 cm radio flux; R–T: Rayleigh–Taylor; PRE: pre-reversal electric field; TPWID: traveling planetary wave ionospheric disturbance; HSA: high solar activity; LSA: low solar activity; CRIRP: China Research Institute of Radio-wave Propagation.

Authors' contributions

WN designed the study, analyzed the data, and wrote the manuscript. GLX and ZZW contributed related analysis on data from HK and GZ. DZH and LLK helped with the text of the paper, particularly with the introduction and comparison with previous works. All coauthors contributed to the revision of the draft manuscript and improvement of the discussion. All authors read and approved the final manuscript.

Author details

[1] School of Physics and Optoelectronic Engineering, Xidian University, Xi'an, Shaanxi 710071, China. [2] National Key Laboratory of Electromagnetic Environment, China Research Institute of Radio-wave Propagation, Qingdao, Shandong 266107, China.

Authors' information

Ning Wang, is currently a Ph.D. student at Xidian University. She also is an Associate Professor at the China Research Institute of Radiowave Propagation. She has authored and coauthored 8 patents and over 15 journal articles. Her current research interests are in ionospheric irregularities and ionosphere radiowave propagation. Dr. Linxin Guo is currently a Professor and Head of the School of Physics and Optoelectronic Engineering Science at Xidian University, China. He has been a Distinguished Professor of the Changjiang Scholars Program since 2014. He has authored and coauthored 4 books and over 300 journal articles. Dr. Zhenwei Zhao is currently a Professor and Chief engineer at the China Research Institute of Radiowave Propagation. His current positions include: Chairman of the ITU-R SG3 in China; Head of the Chinese Delegation of ITU-R SG3; Lead expert for the Asia-Pacific Space Cooperation Organization (APSCO). Dr. Zonghua Ding is currently an Associate Professor at the China Research Institute of Radiowave Propagation. His current research interests are in ionosphere and ionosphere radiowave propagation. Dr. Leke Lin is currently a Professor at the China Research Institute of Radiowave Propagation. He has participated in the activities of the ITU-R study group 3 and has submitted about 40 contributions to the ITU-R SG3.

Acknowledgements

The authors acknowledge the Data Center of the China Research Institute of Radio-wave Propagation for help with ionogram scaling and classification. The authors would like to thank Dr. Shuji Sun and Dr. Tong Xu for proofreading this manuscript. The authors would also like to thank the anonymous referee for the useful comments and suggestions for improving the paper.

Competing interests

The authors declare that they have no competing interests.

Availability of data and materials

Regretfully, the data used in this manuscript cannot be shared because they belonged to the China Research Institute of Radio-wave Propagation (CRIRP).

Consent for publication

Written informed consent was obtained from study participants for participation in the study and for the publication of this report and any accompanying

images. Consent and approval for publication was also obtained from Xidian University and China Research Institute of Radio-wave Propagation.

Ethics approval and consent to participate
Not applicable.

Funding
This research was supported by the National Natural Science Foundation of China (Grant No. 41604129) and the National Key Laboratory Foundation of Electromagnetic Environment (Grant Nos. A171501016, A171601003, A161601002, and B041605003). The funds from Grant No. 41604129 were used for data collection and analysis. The funds from Grant Nos. A171501016, A171601003, A161601002, and B041605003 were used for manuscript preparation.

Publisher's Note

Received: 5 September 2017 Accepted: 24 March 2018
Published online: 16 April 2018

References

Aarons J, Mendillo M, Yantosca R (1994) GPS phase fluctuations in the equatorial region during the MISETA 1994 campaign. J Geophys Res 101:26851–26862

Abadi P, Otsuka Y, Tsugawa T (2015) Effects of pre-reversal enhancement of $E \times B$ drift on the latitudinal extension of plasma bubble in Southeast Asia. Earth Planets Space 67:74. https://doi.org/10.1186/s40623-015-0246-7

Abdu MA, Batista I, Bittencourt JA (1981a) Some characteristics of spread-F at the magnetic equatorial station Fortaleza. J Geophys Res 86:6836–6842

Abdu MA, Bittencourt JA, Batista IS (1981b) Magnetic declination control of the equatorial F region dynamo electric field development and spread F. J Geophys Res 86:11443–11446

Abdu MA, Medeiros RT, Bittencourt JA, Batista IS (1983) Vertical ionization drift velocities and range spread F in the evening equatorial ionosphere. J Geophys Res 88:399–402

Abdu MA, Sobral JHA, Batista IS, Rios VH, Medina C (1998) Equatorial spread-F occurrence statistics in the American longitudes: diurnal, seasonal and solar cycle variations. Adv Space Res 22:851–854

Abdu MA, Souza JR, Batista IS, Sobral JHA (2003) Equatorial spread F statistics and empirical representation for IRI: a regional model for the Brazilian longitude sector. Adv Space Res 31(3):703–716

Abdu MA, Ramkumar TK, Batista IS, Brum CGM, Takahashi H, Reinisch BW, Sobral JHA (2006) Planetary wave signatures in the equatorial atmosphere-ionosphere system, and mesosphere E- and F- region coupling. J Atmos Sol-Terr Phys 68:509–522. https://doi.org/10.1016/j.jastp.2005.03.019

Abdu MA, Alam Kherani E, Batista IS, de Paula ER, Fritts DC, Sobral JHA (2009) Gravity wave initiation of equatorial spread F/plasma bubble irregularities based on observational data from the SpreadFEx campaign. Ann Geophys 27:2607–2622

Alfonsi L, Spogli L, Pezzopane M, Romano V, Zuccheretti E, de Franceschi G, Cabrera MA, Ezquer RG (2013) Comparative analysis of spread-F signature and GPS scintillation occurrences at Tucuman, Argentina. J Geophys Res 118:4483–4502. https://doi.org/10.1002/jgra.50378

Banola S, Pathan BM, Rao DRK, Chandra H (2005) Spectral characteristics of scintillations producing ionospheric irregularities in the Indian region. Earth Planets Space 57:47–59

Booker HG, Wells HG (1938) Scattering of radio waves by the F-region of ionosphere. J Geophys Res 43:249–256

Bowman GG (1974) Ionospheric spread F at Huancayo, sunspot activity and geomagnetic activity. Planet Space Sci 22:1579–1583

Bowman GG (1990) A review of some recent work on midlatitude spread-F occurrence as detected by ionosondes. J Geomagn Geo Electr 42:109–138

Buonsanto MJ, Titheridge JE (1987) Diurnal variations in the flux of ionization above the F2 peak in the northern and southern hemispheres. J Atmos Sol-Terr Phys 49:1093–1105

Chandra H, Rastogi RG (1970) Solar cycle and seasonal variation of spread F near the magnetic equator. J Atmos Terr Phys 32:439–443

Chen HJ, Liu LB, Wan WX, Ning BQ, Lei JL (2006) A comparative study of the bottomside profile parameters over Wuhan with IRI-2001 for 1999-2004. Earth Planets Space 58:601–605

Chou SY, Kuo FS (1996) A numerical study of the wind field effect on the growth and observability of equatorial spread F. J Geophys Res 101:17137–17149

de Abreu AJ, Fagundes PR, Bolzan MJA, Gende M, Brunini C, de Jesus R, Pillat VG, Abalde JR, Lima WLC (2014a) Traveling planetary wave ionospheric disturbances and their role in the generation of equatorial spread-F and GPS phase fluctuations during the last extreme low solar activity and comparison with high solar activity. J Atmos Sol-Terr Phys 117:7–19. https://doi.org/10.1016/j.jastp.2014.05.005

de Abreu AJ, Fagundes PR, Gende M, Bolaji OS, de Jesus R, Brunini C (2014b) Investigation of ionospheric response to two moderate geomagnetic storms using GPS-TEC measurements in the South American and African sectors during the ascending phase of solar cycle 24. Adv Space Res 53:1313–1328. https://doi.org/10.1016/j.asr.2014.02.011

de Abreu AJ, Fagundes PR, Bolzan MJA, de Jesus R, Pillat VG, Abalde JR, Lima WLC (2014c) The role of the traveling planetary wave ionospheric disturbances on the equatorial F region post-sunset height rise during the last extreme low solar activity and comparison with high solar activity. J Atmos Sol-Terr Phys 113:47–57. https://doi.org/10.1016/j.jastp.2014.03.011

de Abreu AJ, Martin IM, Fagundes PR, Venkatesh K, Batista IS, de Jesus R, Rockenback M, Coster A, Gende M, Alves MA, Wild M (2017) Ionospheric F-region observations over American sector during an intense space weather event using multi-instruments. J Atmos Sol-Terr Phys 156:1–14. https://doi.org/10.1016/j.jastp.2017.02.009

de Jesus R, Sahai Y, Guarnieri FL, Fagundes PR, de Abreu AJ, Becker-Guedes F, Brunini C, Gende M, Cintra TMF, de Souza VA, Pillat VG, Lima WLC (2010) Effects observed in the ionospheric F-region in the South American sector during the intense geomagnetic storm of 14 December 2006. Adv Space Res 46:909–920. https://doi.org/10.1016/j.asr.2010.04.031

de Jesus R, Sahai Y, Guarnieri FL, Fagundes PR, de Abreu AJ, Bittencourt JA, Nagatsuma T, Huang CS, Lan HT, Pillat VG (2012) Ionospheric response of equatorial and low latitude F-region during the intense geomagnetic storm on 24-25 August 2005. Adv Space Res 49:518–529. https://doi.org/10.1016/j.asr.2011.10.020

de Jesus R, Sahai Y, Fagundes PR, de Abreu AJ, Brunini C, Gende M, Bittencourt JA, Abalde JR, Pillat VG (2013) Response of equatorial, low- and mid-latitude F-region in the American sector during the intense geomagnetic storm on 24-25 October 2011. Adv Space Res 52:147–157. https://doi.org/10.1016/j.asr.2013.03.017

de Jesus R, Fagundes PR, Coster A, Bolaji OS, Sobral JHA, Batista IS, de Abreu AJ, Venkatesh K, Gende M, Abalde JR, Sumod SG (2016) Effects of the intense geomagnetic storm of September–October 2012 on the equatorial, low- and mid-latitude F region in the American and African sector during the unusual 24th solar cycle. J Atmos Sol-Terr Phys 138–139:93–105. https://doi.org/10.1016/j.jastp.2015.12.015

Deng BC, Huang J, Liu WF, Xu J, Huang LF (2013) GPS scintillation and TEC depletion near the northern crest of equatorial anomaly over South China. Adv Space Res 51:356–365. https://doi.org/10.1016/j.asr.2012.09.008

Devasia CV, Jyoti N, Subbarao KSV, Viswanathan KS, Tiwari D, Sridharan R (2002) On the plausible linkage of thermospheric meridional winds with equatorial spread F. J Atmos Sol-Terr Phys 64:1–12

Fagundes PR, Abalde JR, Bittencourt JA, Sahai Y, Francisco RG, Pillat VG, Lima WLC (2009) *F* layer postsunset height rise due to electric field prereversal enhancement: 2. Traveling planetary wave ionospheric disturbances and their role on the generation of equatorial spread *F*. J Geophy Res Space Phys 114(A12). https://doi.org/10.1029/2009JA014482

Fejer BG, Scherliess L, de Paula ER (1999) Effects of the vertical plasma drift velocity on the generation and evolution of equatorial spread F. J Geophys Res 104:19854–19869

Fukao S, Ozawa Y, Yokoyama T, Yamamoto M (2004) First observations of the spatial structure of F region 3-m-scale field-aligned irregularities with the

equatorial atmosphere radar in Indonesia. J Geophys Res 109:A02304. https://doi.org/10.1029/2003JA010096
Hu LH, Ning BQ, Li GZ, Li M (2014) Observations on the field-aligned irregularities using Sanya VHF radar: 4. June solstitial F region echoes in solar minimum. Chinese J Geophys 57(1):1–9
Huang CS, Kelley MC, Hysell DL (1993) Nonlinear Rayleigh-Taylor instabilities, atmospheric gravity waves and equatorial spread F. J Geophys Res 98:15631–15642
Joshi LM, Patra AK, Rao SVB (2013) Low-latitude Es capable of controlling the onset of equatorial spread F. J Geophys Res 118:1170–1179. https://doi.org/10.1002/jgra.50189
Jyoti N, Devasia CV, Sridharan R, Diwakar Tiwari (2004) Threshold height $(h'F)_c$ for the meridional wind to play a deterministic role in the bottom side equatorial spread F and its dependence on solar activity. Geophys Res Lett 31:L12809. https://doi.org/10.1029/2004GL019455
Liu GQ, Shen H (2017) A severe negative response of the ionosphere to the intense geomagnetic storm on March 17, 2015 observed at mid- and low-latitude stations in the China zone. Adv Space Res 59:2301–2312. https://doi.org/10.1016/j.asr.2017.02.021
Liu JH, Liu LB, Wan WX, Zhang SR (2004a) Modeling investigation of ionospheric storm effects over Millstone Hill during August 4-5, 1992. Earth Planets Space 56:903–908
Liu LB, Wan WX, Lee CC, Ning BQ, Liu JY (2004b) The low latitude ionospheric effects of the April 2000 magnetic storm near the longitude 120°E. Earth Planets Space 56:607–612
Madhav Haridas MK, Manju G, Kumar Pant T (2013) First observational evidence of the modulation of the threshold height h′Fc for the occurrence of equatorial spread F by neutral composition changes. J Geophys Res 118:3540–3545. https://doi.org/10.1002/jgra.50331
Manju G, Madhav Haridas MK (2015) On the equinoctial asymmetry in the threshold height for the occurrence of equatorial spread F. J Atmos Sol-Terr Phys 124:59–62. https://doi.org/10.1016/j.jastp.2015.01.008
Manju G, Devasia CV, Sridharan R (2007) On the seasonal variations of the threshold height for the occurrence of equatorial spread F during solar minimum and maximum years. Ann Geophys 25:855–861
Maruyama T (1988) A diagnostic model for equatorial spread F 1. Model description and application to electric field and neutral winds effects. J Geophys Res 93:14611–14622
Maruyama T, Matuura N (1984) Longitudinal variability of annual changes in activity of equatorial spread F and plasma bubbles. J Geophys Res 89:10903–10912
Maruyama T, Saito S, Kawamura M, Nozaki K, Krall J, Huba JD (2009) Equinoctial asymmetry of a low-latitude ionosphere-thermosphere system and equatorial irregularities: evidence for meridional wind control. Ann Geophys 27:2027–2034
Mo XH, Zhang DH, Goncharenko L, Zhang SR, Hao YQ, Xiao Z, Pei JZ, Yoshikawa A, Chau H (2017) Meridional movement of northern and southern equatorial ionization anomaly crests in the East-Asian sector during 2002-2003 SSW. Sci China Earth Sci 60:776–785. https://doi.org/10.1007/s11430-016-0096-y
Narayanan VL, Sau S, Gurubaran S, Shiokawa K, Balan Nanan, Emperumal K, Sripathi S (2014) A statistical study of satellite traces and evolution of equatorial spread F. Earth Planets Space 66:160. https://doi.org/10.1186/s40623-014-0160-4
Narayanan VL, Gurubaran S, Berlin Shiny MB, Emperumal K, Patil PT (2017) Some new insights of the characteristics of equatorial plasma bubbles obtained from Indian region. J Atmos Sol-Terr Phys 156:80–86. https://doi.org/10.1016/j.jastp.2017.03.006
Ossakow SL (1981) Spread F theories - a review. J Atmos Sol-Terr Phys 43:437–452
Rungraengwajiake S, Supnithi P, Tsugawa T, Maruyama T, Nagatsuma T (2013) The variation of equatorial spread-F occurrences observed by ionosondes at Thailand longitude sector. Adv Space Rec 52:1809–1819. https://doi.org/10.1016/j.asr.2013.07.041
Scherliess L, Fejer BG (1999) Radar and satellite global equatorial F region vertical drift model. J Geophys Res 104:6829–6842
Smith JM, Rodrigues FS, de Palua ER (2015) Radar and satellite investigations of equatorial evening vertical drifts and spread F. Ann Geophys 33:1403–1412. https://doi.org/10.5194/angeo-33-1403-2015
Sripathi S, Kakad B, Bhattacharyya A (2011) Study of equinoctial asymmetry in the Equatorial Spread F (ESF) irregularities over Indian region using multi-instrument observations in the descending phase of solar cycle 23. J Geophys Res 116:A11302. https://doi.org/10.1029/2011JA016625
Stoneback RA, Heelis RA, Burrell AG, Coley WR, Fejer BG, Pacheco E (2011) Observations of quiet time vertical ion drift in the equatorial ionosphere during the solar minimum period of 2009. J Geophys Res 116:A12327. https://doi.org/10.1029/2011JA016712
Sukanta Sau, Narayanan VL, Gurubaran S, Ghodpage Rupesh N, Patil PT (2017) First observation of interhemispheric asymmetry in the EPBs during the St. Patrick's Day geomagnetic storm of 2015. J Geophys Res 122:6679–6688. https://doi.org/10.1002/2017JA024213
Upadhayaya AK, Gupta S (2014) A statistical analysis of occurrence characteristics of spread-F irregularities over Indian region. J Atmos Sol-Terr Phys 112:1–9. https://doi.org/10.1016/j.jastp.2014.01.019
Wan WX, Xu JY (2014) Recent investigation on the coupling between the ionosphere and upper atmosphere. Sci China Earth Sci 57:1995–2012. https://doi.org/10.1007/s11430-014-4923-3
Wang Z, Shi JK, Torkar K, Wang GJ, Wang X (2014) Correlation between ionospheric strong range spread F and scintillations observed in Vanimo station. J Geophys Res 119:8578–8585. https://doi.org/10.1002/2014JA020447
Xiao Z, Zhang TH (2001) A theoretical analysis of global characteristics of spread-F. Chin Sci Bull 46:1593–1594
Xiong C, Luhr H, Ma SY, Stolle C, Fejer BG (2012) Features of highly structured equatorial plasma irregularities deduced from CHAMP observations. Ann Geophys 30:1259–1269. https://doi.org/10.5194/angeo-30-1259-2012
Xu T, Wu ZS, Hu YL, Wu J, Suo YC, Feng J (2010) Statistical analysis and model of spread F occurrence in China. Sci China Tech Sci 53:1725–1731. https://doi.org/10.1007/s11431-010-3169-3
Zhang Y, Wan W, Li G, Liu L, Hu L, Ning B (2015) A comparative study of GPS ionospheric scintillations and ionogram spread F over Sanya. Ann Geophys 33:1421–1430. https://doi.org/10.5194/angeo-33-1421-2015